

Computer-assisted diagnosis of breast lesions based on IVIM and non Gaussian diffusion MRI

Mami Iima¹, Masako Kataoka¹, Masaki Umehana², Yuto Nakanishi², Takayuki Ito², Kojiro Yano³, Shotaro Kanao¹, Kaori Togashi¹, and Denis Le Bihan^{4,5}

¹Diagnostic Imaging and Nuclear Medicine, Kyoto University Graduate School of Medicine, Kyoto, Kyoto, Japan, ²Kyoto University Faculty of Medicine, Kyoto, Kyoto, Japan, ³Information Science and Technology, Osaka Institute of Technology, Hirakata, Osaka, Japan, ⁴Human Brain Research Center, Kyoto University Graduate School of Medicine, Kyoto, Kyoto, Japan, ⁵Neurospin, CEA Saclay, Gif-sur-Yvette, Ile-de-France, France

Targeted audience: Scientists and clinicians interested in perfusion and diffusion MRI with application to breast cancer

Introduction: Intravoxel incoherent motion (IVIM) imaging (1) has undergone a striking revival recently, especially in cancer imaging, as it has the potential to provide information on tissue microvasculature (e.g. flowing blood fraction, a key parameter for angiogenesis (2,3)) without contrast agents, an alternative for perfusion MRI. Furthermore, IVIM MRI also gives access to non-Gaussian diffusion parameters (e.g. mean diffusion and kurtosis) which provide information on tissue microstructure (4). We have implemented an algorithm which enables automatic classification of breast tumor types (i.e. benign or malignant) based on 3 IVIM parameters. This computer-assisted diagnostic tool has been evaluated in a series of patients with breast lesions.

Material and Methods: This prospective study included 36 (31 malignant and 5 benign) patients suspected of breast tumors with a diameter of more than 1 cm, histopathologically diagnosed by biopsy. Breast MRI was performed using a 3-T system (Trio, B17; Siemens AG) equipped with a dedicated 16-channel breast array coil. The following images were obtained after localizers were acquired: 1. bilateral fat-suppressed T2-weighted images 2. Diffusion-weighted images (single shot EPI along three orthogonal axes (5); 16 b values of 0, 5, 10, 20, 30, 50, 70, 100, 200, 400, 600, 800, 1000, 1500, 2000, 2500 sec/mm²; repetition time/echo time, 4,600/86 ms; flip angle, 90°; field of view, 160×300 mm²; matrix, 80×166; slice thickness, 3.0 mm; and acquisition time, 3 min 55 sec); 3. Dynamic contrast enhanced (DCE) images: non-fat-suppressed T1-weighted images; and fat-suppressed T1-weighted dynamic contrast-enhanced images obtained using a 3-dimensional fat-suppressed gradient-echo sequence (repetition time/echo time, 3.7/1.36 ms; flip angle, 15°; field of view, 330 × 330 mm²; matrix, 346×384; slice thickness, 1 mm; and acquisition time, 60 s). The fat-suppressed T1-weighted dynamic contrast-enhanced images were acquired before and 3 times (0–1, 1–2, and 5–6 min) after contrast injection.

IVIM data were analyzed in 3 steps on a voxel-by-voxel basis. First, the diffusion component of the signal (signal attenuation, S/S₀, for b values > 200s/mm²) was corrected for noise-floor effects and fitted using a kurtosis diffusion model (diffusion coefficient, ADC₀, and kurtosis, K)(6,7).

$$S/S_0 = \exp[-bADC_0 + K(bADC_0)^2/6] \quad [1]$$

Second, the diffusion component was subtracted from the signal acquired with b<200s/mm² and the remaining signal was fitted using the IVIM model¹ to get estimates of the flowing blood fraction, f_{IVIM}, and the pseudodiffusion, D*. Last, a parametric (diagnostic) map was generated by ascribing each voxel a value from 0 to 3 according to the number of parameters (f_{IVIM}, ADC₀, K) falling beyond a given threshold. Those thresholds for each individual parameter (K>0.80, ADC₀<1.40 × 10⁻³mm²/s, f_{IVIM}>2.07%) have been previously established from a retrospective study³ based on 21 patients (15 malignant and 6 benign tumors) with the same acquisition parameters and processing, but on a Region-of-Interest basis, using a ROC analysis under the condition of 100 % sensitivity for malignancy and 100% negative predictive value for benign tumors (Fig.1: ROC analysis for ADC₀, K and f_{IVIM} from the retrospective study). Diagnostic maps were displayed using a color-scale (3: red, 2: orange, 1: green, 0: blue). Red and orange voxels were classified as “malignant likely” while green and blue voxels were deemed “benign likely”. To account for tumor inhomogeneities diagnosis was determined from the voxels with the highest value present within the lesion, as delineated manually, avoiding necrotic or hemorrhagic parts.

Results: Examples of lesion parametric maps are given in Fig.2 (malignant; invasive ductal carcinoma) and Fig.3 (benign; fibroadenoma). Parametric maps of ADC₀, K and f_{IVIM} are also shown to illustrate tumor heterogeneity. Central necrosis is suspected in Figure 2 (high ADC₀, low K and f_{IVIM}). Orange and red pixels (malignancy likely) are located only at the periphery of the tumor. In Fig.3, the dorsal side of the tumor is highly enhanced on the early phase of CE image and exhibits high f_{IVIM} values, but the tumor is classified as benign (blue/green pixels) based on the ADC₀ and K values. The overall performance of the algorithm for our patient series is shown in Table 1.

Sensitivity was 97 (83-100) %, specificity 100 (48-100) %, PPV 100 (88-100) %, and NPV was 83 (36-100) %. Those values were much improved when compared to the performance of each separate parameter considered separately, especially f_{IVIM}.

Discussion: Although results look very promising the performance of this computer-assisted diagnosis tool will have to be validated on a much larger cohort of patients with a broader range of lesion types. Especially, some benign tumors, such as fibroadenoma (Fig.3), present high perfusion values (8), which could result in false positive depending on the ADC₀ and K values. Small lesions (<1cm) were excluded in our study. Such small lesions would benefit from a 3D cluster analysis to increase voxel counts. Also, identification and delineation of some tumor parts (necrosis, hemorrhage) requires expertise from a trained radiologist.

Conclusion: Although more work remains for further development and validation this computer-assisted tool has the potential to give a semi-automatic diagnosis of breast lesions with high accuracy without the need for contrast agents, an important benefit for patients exposed to the risk of Nephrogenic Systemic Fibrosis (NSF). Furthermore, the diagnostic maps may provide guidance for biopsy location more accurately than from CE images.

References:

- (1) Le Bihan D, Breton E, Lallemand D, et al. Radiology. 1988;168:497-505.
- (2) Sigmund E. E, G. Y. Cho, S. Kim, et al. MRM 2011;65:1437–1447.
- (3) Iima M, Kataoka M, Le Bihan D, et al. 21th Proceedings of ISMRM, Salt Lake City, U.S.A., 2013, p.3383.
- (4) Le Bihan D. Radiology 2013; 268:318–322.
- (5) Morelli JN, Runge VM, Feiweier T et al. Invest Radiol. 2010;45:29-35.
- (6) Chabert S et al. 12th Proceedings of ISMRM, Kyoto, Japan, 2004, p.1238.
- (7) Jensen JH et al. NMR in Biomedicine. 2010;23:698-710.
- (8) Wurdinger S et al. AJR Am J Roentgenol. 2005 185:1317-21.

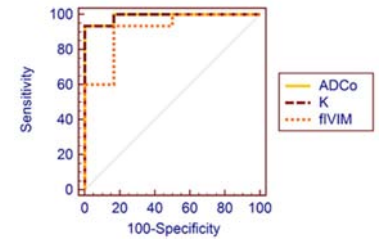


Figure 1

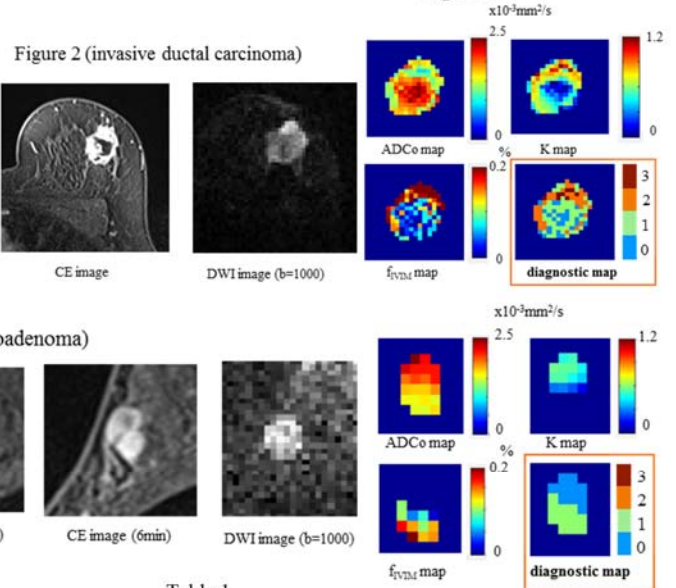


Table 1

	Malignant	Benign
Test Positive for Malignancy	30	0
Test Negative	1	5